

1 **Rational design of proteins that exchange on functional timescales**

2

3 James A. Davey,<sup>†</sup> Adam M. Damry,<sup>†</sup> Natalie K. Goto<sup>\*</sup> & Roberto A. Chica<sup>\*</sup>

4

5 **Affiliations:**

6 Department of Chemistry and Biomolecular Sciences, University of Ottawa, Ottawa, Ontario,

7 K1N 6N5, Canada

8

9 \*Correspondence to: E-mail: [rchica@uottawa.ca](mailto:rchica@uottawa.ca), [ngoto@uottawa.ca](mailto:ngoto@uottawa.ca)

10 <sup>†</sup> These authors contributed equally to this work

11

12 **Abstract**

13 Proteins are intrinsically dynamic molecules that can exchange between multiple  
14 conformational states, enabling them to carry out complex molecular processes with extreme  
15 precision and efficiency. Attempts to design novel proteins with tailored functions have mostly  
16 failed to yield efficiencies matching those found in nature because standard methods do not allow  
17 for the design of exchange between necessary conformational states on a functionally-relevant  
18 timescale. Here, we develop a broadly-applicable computational method to engineer protein  
19 dynamics that we term *meta*-multistate design. We used this methodology to design spontaneous  
20 exchange between two novel conformations introduced into the global fold of Streptococcal protein  
21 G domain  $\beta$ 1. The designed proteins, named DANCERs, for *Dynamic And Native Conformational*  
22 *ExchangeRs*, are stably folded and exchange between predicted conformational states on the  
23 millisecond timescale. The successful introduction of defined dynamics on functional timescales  
24 opens the door to new applications requiring a protein to spontaneously access multiple  
25 conformational states.

## 26 **Main Text**

27 Proteins have found widespread application in research, industry, and medicine because  
28 they can mediate complex molecular processes with extreme precision and efficiency. Even so,  
29 continued engineering of proteins with tailored functions is essential to enable novel  
30 biotechnological applications. Computational protein design (CPD) has enjoyed considerable  
31 success in creating protein sequences that stably adopt a single targeted structure (1-5). However,  
32 attempts to use these methods to generate proteins that can carry out specific functions have mostly  
33 failed to match the efficiencies that are found in nature (6-9), suggesting that fundamental aspects  
34 of protein structure that are not currently considered in design strategies must be incorporated in  
35 order to create proteins that can approach the efficacy of naturally occurring systems. One such  
36 feature is dynamics, which have been shown to be essential for many complex protein functions  
37 (10-13). The development of a general strategy for the rational design of protein sequences  
38 displaying predictable dynamic properties has great potential to expand the range and functionality  
39 of designed proteins, paving the way to applications that are currently inaccessible using natural  
40 proteins.

41 The rational design of protein dynamics requires the prediction of sequences that can adopt  
42 the necessary conformational states for exchange. The recent development of multistate design  
43 (MSD) approaches applicable to large structural ensembles (14-16) has provided a method for the  
44 evaluation of protein sequence energies in the context of a large number of possible conformational  
45 states. Thus, MSD can in principle be used to assess the energy landscape of a target protein and  
46 identify sequences that can exchange between distinct states. However, introduction of functionally  
47 relevant conformational exchange into a stable protein fold is a difficult design problem as it  
48 requires *a priori* knowledge of the structural features of the relevant conformational states for  
49 dynamic exchange, including the endpoint structures and intermediate states that the protein must

50 adopt as it undergoes this conformational transition, which are often unknown. In addition, the  
51 multivariable optimization of sequences across many conformational states presents a significant  
52 computational challenge, since sequences must be designed that not only satisfy stability  
53 requirements for multiple target structures, but also yield an energy profile that would allow  
54 exchange between structures to occur on a functionally relevant timescale.

55         Herein, we have developed a general procedure that addresses these challenges and enables  
56 the rational design of protein dynamics, which we termed *meta*-MSD (Fig. 1). *Meta*-MSD enables  
57 the evaluation of protein energy landscapes in order to predict sequences able to spontaneously  
58 exchange between specific states. Unlike standard MSD methodologies where states are defined  
59 by the user prior to calculation (e.g., target and off-target states), *meta*-MSD instead assigns the  
60 identity of the states based on their structural characteristics after rotamer optimization, enabling  
61 the unbiased prediction of the preferred state for each sequence, along with an evaluation of the  
62 relative energies of every state that the sequence can stably adopt. We applied this methodology to  
63 the design of sequences that adopt the global fold of Streptococcal protein G domain  $\beta$ 1 (G $\beta$ 1) and  
64 spontaneously exchange between two conformations that have not been previously observed for  
65 this fold. The designed dynamic G $\beta$ 1 variants, termed DANCERs, for *Dynamic And Native*  
66 *Conformational ExchangeRs*, were shown to be stably folded and to exchange between the  
67 predicted conformational states on the millisecond timescale.

68

## 69 **Computational design of a protein energy landscape**

70         A dynamic protein that spontaneously interconverts between two distinct conformational  
71 states adopts a continuum of unique configurations during exchange. However, the energy  
72 landscape is complex and the range of configurations that are sampled over the course of exchange  
73 cannot be completely defined. Nevertheless, it should be possible to engineer a user-defined

74 exchange trajectory by identifying sequences that stabilize configurations having structural  
75 characteristics postulated to facilitate this exchange. To simplify the exchange reaction coordinate,  
76 the conformational landscape can be conceptually divided into three states: a major, a minor, and  
77 a transition state (Fig. S1). In the context of this work, we treat each of these states as a collection  
78 of unique configurations that we will refer to as microstates. Microstates are generated by  
79 optimizing rotamers for predefined sequences on an ensemble of backbone templates using MSD,  
80 which also returns an energy value for each microstate that reflects its predicted stability (Fig. 1,  
81 panels I–III). Following MSD, microstates are partitioned into their corresponding states according  
82 to their structural features (Fig. 1, panel IV), and the energy of each state is calculated from the  
83 energy of its constituent microstates. Evaluation of relative energies between each state then allows  
84 prediction of the exchange profile for each sequence, allowing identification of sequences that  
85 would give rise to static or dynamic G $\beta$ 1 folds (Fig. 1, panels V–VI). We call this framework *meta-*  
86 *MSD* because both state and dynamic behavior are assigned after rotamer optimization by MSD.  
87 *Meta-MSD* can be used to identify sequences that can stably populate the two target states, with a  
88 transition state barrier that is small enough to allow interconversion between these two states,  
89 enabling the rational design of dynamics.

90 To validate our *meta-MSD* framework, we targeted the introduction of millisecond  
91 timescale exchange into the G $\beta$ 1 structure. Native G $\beta$ 1 is rigid on this timescale (17), with a small  
92 size (56 amino acids) that facilitates characterization of its dynamic properties at atomic resolution.  
93 Additionally, G $\beta$ 1 possesses a single tryptophan residue (Trp43) that in high-resolution structures  
94 of G $\beta$ 1 and its natively folded variants (18-28) exclusively occupies a single side-chain  
95 conformation with  $\chi_1$  and  $\chi_2$  dihedrals of  $-74 \pm 9^\circ$  and  $+75 \pm 11^\circ$ , respectively. We name this  
96 conformation +g(-) due to its positive  $\chi_2$  dihedral angle and its *gauche*(-)  $\chi_1$  dihedral (Fig. S2). In  
97 G $\beta$ 1, the Trp43 side chain is mostly solvent inaccessible, making intimate contacts with several

98 residues that comprise the hydrophobic core. This makes it an attractive target for the design of  
99 conformational exchange, with one state being buried, and the other being excluded from the  
100 hydrophobic core in a solvent-exposed conformation that should be straightforward to distinguish  
101 spectroscopically. In addition, exchange between a core-buried and solvent-exposed state is  
102 expected to involve the disruption of side-chain interactions that should increase the kinetic barrier  
103 separating states, while not requiring large-scale changes in backbone structure that could prove  
104 kinetically inaccessible (29). Moreover, with exchange of the tryptophan side chain being set as  
105 our target for the design of dynamics, tryptophan side-chain dihedral angles provide a convenient  
106 metric for the assignment of microstates to one of the target states defined in our *meta*-MSD  
107 approach.

108       Using *meta*-MSD, we designed G $\beta$ 1 sequences that could adopt the native fold and also  
109 undergo conformational exchange between a state where the Trp43 indole is solvent-exposed  
110 [-g(+)] and a state where the indole is sequestered from the solvent in the hydrophobic core [-  
111 g(-)] (Fig. S3). Notably, we avoided selection of the native Trp43 conformation [+g(-)] for the  
112 core-buried state, since CPD has a tendency to overemphasize the stability of the native rotamer  
113 relative to non-native configurations (30). A final and particularly critical aspect of our  
114 conformational exchange design was the definition of an intermediate state with the Trp43 side  
115 chain in the  $-t$  conformation, since this state is necessary to provide a model of transiently  
116 populated microstates that are sampled along the reaction coordinate. Use of the  $-t$  conformation  
117 as a proxy of the transition state thus allowed estimation of kinetic barriers between states, enabling  
118 the elimination of sequences predicted to stably adopt two end-states separated by large kinetic  
119 barriers that would not exchange on functionally relevant timescales.

120       To ensure adequate sampling of the range of structures that may be required to  
121 accommodate the designed conformational exchange, an ensemble of 12,648 templates was

122 prepared using a combination of several template generation procedures (Fig. S4, Table S1, and SI  
123 Text). Using this ensemble, MSD was performed to optimize rotamers for a library of 1,296 G $\beta$ 1  
124 sequences comprising combinations of core-residue mutations (Fig. S5) that were previously  
125 reported to result in folded G $\beta$ 1 variants (14). MSD thus yielded >16 million microstates and  
126 corresponding energies, allowing for approximation of the accessible conformational landscape of  
127 Trp43 in the native G $\beta$ 1 fold.

128 Sequences having a Boltzmann-weighted average of MSD energies greater than that of the  
129 wild-type sequence are less likely to adopt a stable G $\beta$ 1 fold (15) and were therefore eliminated  
130 from the *meta*-MSD analysis. For the remaining 195 sequences, each microstate was classified as  
131 being in a core-buried [-g(-)], solvent-exposed [-g(+)], or intermediate [-*l*] state based on the  $\chi_1$   
132 and  $\chi_2$  dihedrals of the Trp43 side chain. The energy of each of these states was determined for  
133 every sequence by taking the energy of the most stable microstate assigned to each state. State  
134 energies were used to construct an energy profile for each sequence (Fig. 1, panel V), enabling us  
135 to identify 35 sequences predicted to allow conformational exchange between the target core-  
136 buried and solvent-exposed conformations (SI Text), of which four were selected for experimental  
137 characterization (Table 1, DANCER proteins).

138

### 139 **Experimental characterization**

140 Although the four DANCER proteins each contained between five and six mutations,  
141 representing approximately 10% of the G $\beta$ 1 total sequence length, they expressed as soluble  
142 monomers (Fig. S6), adopted the native G $\beta$ 1 fold (Fig. S7), and were folded at room temperature  
143 (Fig. S8, Table S2). Chemical denaturation experiments (Fig. S9) could be fit to a two-state model  
144 with *m*-values similar to that of the wild type (Table S2), indicating a similar level of protein surface  
145 exposed to solvent upon unfolding (31). In addition, all DANCER variants have unfolding free

146 energies that are 1.5 kcal/mol and higher (Table 1), confirming that they are stably folded at room  
147 temperature. Solution NMR was used to assess the dynamic properties of DANCER proteins, with  
148  $^1\text{H}$ - $^{15}\text{N}$  heteronuclear single quantum coherence (HSQC) spectra showing immediate evidence that  
149 DANCER proteins exist in two distinct conformational states (Fig. S10). Specifically, spectra for  
150 DANCER-1, DANCER-2, and DANCER-3 all showed the presence of a minor species not seen in  
151 spectra of wild-type G $\beta$ 1 (Fig. S11). The only exception was DANCER-0, which instead showed  
152 significant peak broadening, suggesting that it is dynamic on a faster timescale (32).

153 Using  $^1\text{H}$ - $^{15}\text{N}$  HSQC ZZ-exchange experiments (Fig. 2 and S12), we confirmed that the  
154 minor species in DANCER-1, DANCER-2, and DANCER-3 is an alternate state of G $\beta$ 1  
155 undergoing exchange with the major species. Mixing-time dependent changes in peak intensities  
156 acquired over a range of temperatures could be fit to kinetic and thermodynamic parameters of  
157 exchange for DANCER-1 and DANCER-3 (Table 1, Fig. S13), confirming that conformational  
158 exchange is occurring on the millisecond timescale. DANCER-1 exhibits approximately 10-fold  
159 faster exchange than DANCER-3, with an activation barrier that is 1.75 kcal/mol smaller in  
160 magnitude. Conformational exchange was also observed for DANCER-2, although the small  
161 population of the minor state (< 10%) prevented quantitative measurement of kinetic parameters  
162 for this mutant.

163 To obtain structural evidence that the two conformations sampled by our dynamic G $\beta$ 1  
164 variants matched structural states predicted by *meta*-MSD, solution NMR was used to solve the  
165 structure of the major state of DANCER-2 (Fig. 3A, Table S3). As predicted, this structure shows  
166 a native G $\beta$ 1 fold with  $\chi_1$  and  $\chi_2$  dihedrals for Trp43 that correspond to the solvent-exposed -g(+)   
167 conformation (Table 2). However, there was also a secondary network of low intensity NOEs  
168 involving the Trp43 side chain that were not compatible with this structure, but could be used to  
169 determine a structural model for the alternate, minor state (SI Text). According to this model (Fig.



170 3B, Table S3), the configuration of Trp43 in the minor state is in the core-buried  $-g(-)$  state (Table  
171 2), as predicted by *meta*-MSD. Taken together, these data demonstrate that we have successfully  
172 designed a sequence that adopts the G $\beta$ 1 fold while undergoing conformational exchange on a  
173 millisecond timescale between two conformational states that have not previously been observed,  
174 but were the targets of our design protocol.

175 To illustrate the reliability of our *meta*-MSD predictions, we also characterized the structure  
176 and dynamics of DANCER-1 and DANCER-3. While the exchange parameters for these mutants  
177 made it impractical to attempt structure determination,  $^1\text{H}$ - $^{15}\text{N}$  HSQC spectra of the major species  
178 showed similarities with those of other structurally characterized variants, suggesting a high degree  
179 of structural similarity with these states. Specifically, the DANCER-1 spectrum shows only small  
180 chemical shift differences from that of DANCER-2 (Fig. 4A), suggesting that the major species of  
181 DANCER-1 also contains Trp43 in the solvent-exposed  $-g(+)$  state. Likewise, the  $^1\text{H}$ - $^{15}\text{N}$  HSQC  
182 spectrum for DANCER-3 was highly similar to that of a variant that we determined to  
183 thermodynamically and kinetically favor the  $-g(+)$  state as predicted by *meta*-MSD (Fig. 4B),  
184 called NERD-S, for *Non-Exchanging Rigid Design with a Solvent-exposed* Trp43 side chain (SI  
185 Text, Fig. 3C, Tables 1, 2, and S3). Therefore in all three of the mutants predicted by *meta*-MSD  
186 to be dynamic for which structural information could be obtained, the major conformation was the  
187 G $\beta$ 1 structure with Trp43 being in the solvent-exposed  $-g(+)$  state.

188 Insight into the minor states being sampled in the conformational exchange exhibited by  
189 DANCER-1 and DANCER-3 was provided by  $^1\text{H}$ - $^{15}\text{N}$ -NOE correlations involving the Trp43  
190 indole NH proton. DANCER-1 and DANCER-3 spectra show NOE correlations (Fig. S14) to  
191 similar regions of the protein as was observed in DANCER-2 (Fig. 4C), consistent with exchange  
192 between core-buried  $-g(-)$  and solvent-exposed  $-g(+)$  states. Furthermore, comparison of NOEs  
193 involving the Trp43 indole NH proton confirmed that these correlations do not correspond to the

194 core-buried state found in the wild-type structure [+g(-)] (SI text, Fig. S15). Taken together, our  
195 NMR results confirm that the Trp43 residues of DANCER-1 and DANCER-3 exchange between  
196 the solvent-exposed -g(+) and core-buried -g(-) conformations that were the targets of our design,  
197 and also suggest that exchange is achieved via a coordinated change in side-chain configurations  
198 for a triad of aromatic residues (Phe34, Trp43, Phe45) in a process we have termed an aromatic  
199 relay (SI text, Fig. S16).

200

## 201 **Discussion**

202       The *meta*-MSD framework described here enabled the rational design of G $\beta$ 1 variants that  
203 spontaneously exchange between two predefined states on the millisecond timescale without the  
204 need for an external stimulus to induce exchange. To our knowledge, this work represents the first  
205 successful application of CPD to engineer a specific mode of conformational exchange into a stable  
206 protein fold. Although a previous CPD-based design generated a protein capable of reversible  
207 exchange between coiled-coil trimer and zinc-finger folds ( $\delta$ ), this relied on the presence of a metal  
208 that was critical for the formation of the zinc finger structure. In that case, it was possible to design  
209 exchange by simultaneously minimizing the sum of the sequence energies across both folds. In  
210 contrast, to design conformational exchange between two states in the absence of a ligand or other  
211 external stimulus, we found that it was essential to explicitly consider both the relative energies  
212 between the two target end-states ( $\Delta E_{\text{eq}}$ ) and the barrier to conformational exchange ( $\Delta E^{\ddagger}$ ).  
213 Without estimation of both of these energy differences, it would not have been possible to  
214 distinguish between dynamic (DANCER) and static (NERD) sequences (e.g., both  $\Delta E_{\text{eq}}$  and  $\Delta E^{\ddagger}$   
215 values for DANCERs were lower than for NERDs and wild-type G $\beta$ 1, Table 1).

216       Another key advantage arising from our utilization of a *meta*-analysis-based design strategy  
217 is that it enabled the use of a significantly larger structural ensemble than has previously been

218 utilized in MSD approaches. This was of critical importance, since we found that the full  
219 complement of seed structure and ensemble generation strategies used in our framework was  
220 required to approximate the energy landscape of the designed exchange trajectory with enough  
221 accuracy to predict DANCER variants (SI Text, Table S4). In addition, the large ensemble size  
222 made it possible to design exchange in the absence of specific structures corresponding to each  
223 end-state, in contrast with the metal-triggered conformational exchange that was previously  
224 designed using available crystal structures as templates for the two end-states (8).

225         Importantly, our results show that the introduction of dynamics on the millisecond timescale  
226 cannot be achieved via a single mutation and that instead dynamics is conferred through subtle  
227 interactions across a network of residues. For example, the A34F mutation, which was previously  
228 shown to induce dimerization of G $\beta$ 1 without altering the Trp43 conformation (27, 33), is common  
229 to all DANCER proteins and an integral component of the aromatic relay that underlies exchange  
230 (Fig. S16). However, this mutation alone is not sufficient to introduce dynamics into the G $\beta$ 1 fold,  
231 since the variant NERD-S also possesses this mutation but does not undergo exchange on the  
232 millisecond timescale (Table 1). Introduction of the conservative and isosteric I39L mutation into  
233 the NERD-S sequence appears to be sufficient to introduce the targeted conformational exchange,  
234 giving rise to the dynamic variant DANCER-3. These results highlight the challenges of attempting  
235 to infer dynamics from simple sequence characteristics, and demonstrate the power of *meta*-MSD  
236 to design conformational exchange into proteins even without prior knowledge of the mechanism  
237 of exchange.

238

## 239 **Conclusion**

240         The *meta*-MSD framework presented here is in principle applicable to the design of specific  
241 conformational exchange into any globular protein. In the future, *meta*-MSD could also be used to

242 design proteins with functions that rely on the ability to spontaneously access more than one  
243 conformational state (*e.g.* open and closed states of an enzyme to facilitate substrate binding and  
244 catalysis, respectively). Alternatively, *meta*-MSD could be used to enrich functionally relevant but  
245 low occupancy states from an ensemble of dynamic configurations to improve function (34).  
246 Moreover, while we have demonstrated the introduction of dynamics into a rigid protein,  
247 dampening of dynamics should in principle also be possible, as demonstrated by our design of  
248 NERD-C and NERD-S. This potential for *meta*-MSD to be used for the rigidification of highly  
249 dynamic regions in proteins without adversely affecting the overall structure, in effect imitating  
250 conformational selection *in silico*, opens the door to the design of proteins with a wider range of  
251 functions than previously possible.

252

253 **Data Availability.** Structure coordinates have been deposited in the Protein Data Bank with  
254 accession codes 5UB0 (NERD-C), 5UBS (NERD-S), 5UCE (major state of DANCER-2), and  
255 5UCF (minor state of DANCER-2). NMR data has been deposited in the Biological Magnetic  
256 Resonance Data Bank with accession codes 30220 (NERD-C), 30221 (NERD-S), 30222  
257 (DANCER-2), 27030 (DANCER-0), 27031 (DANCER-1), and 27032 (DANCER-3).

258

259 **References**

- 260 1. B. I. Dahiyat, S. L. Mayo, De novo protein design: fully automated sequence selection.  
261 *Science* **278**, 82-87 (1997).
- 262 2. B. Kuhlman, G. Dantas, G. C. Ireton, G. Varani, B. L. Stoddard, D. Baker, Design of a  
263 novel globular protein fold with atomic-level accuracy. *Science* **302**, 1364-1368 (2003).
- 264 3. N. Koga, R. Tatsumi-Koga, G. Liu, R. Xiao, T. B. Acton, G. T. Montelione, D. Baker,  
265 Principles for designing ideal protein structures. *Nature* **491**, 222-227 (2012).

- 266 4. E. Marcos, B. Basanta, T. M. Chidyausiku, Y. Tang, G. Oberdorfer, G. Liu, G. V. Swapna,  
267 R. Guan, D. A. Silva, J. Dou, J. H. Pereira, R. Xiao, B. Sankaran, P. H. Zwart, G. T.  
268 Montelione, D. Baker, Principles for designing proteins with cavities formed by curved beta  
269 sheets. *Science* **355**, 201-206 (2017).
- 270 5. S. M. Malakauskas, S. L. Mayo, Design, structure and stability of a hyperthermophilic  
271 protein variant. *Nat Struct Biol* **5**, 470-475 (1998).
- 272 6. L. Jiang, E. A. Althoff, F. R. Clemente, L. Doyle, D. Röthlisberger, A. Zanghellini, J. L.  
273 Gallaher, J. L. Betker, F. Tanaka, C. F. Barbas, 3rd, D. Hilvert, K. N. Houk, B. L. Stoddard,  
274 D. Baker, De novo computational design of retro-aldol enzymes. *Science* **319**, 1387-1391  
275 (2008).
- 276 7. S. Bjelic, L. G. Nivón, N. Çelebi-Ölçüm, G. Kiss, C. F. Rosewall, H. M. Lovick, E. L.  
277 Ingalls, J. L. Gallaher, J. Seetharaman, S. Lew, G. T. Montelione, J. F. Hunt, F. E. Michael,  
278 K. N. Houk, D. Baker, Computational design of enone-binding proteins with catalytic  
279 activity for the Morita-Baylis-Hillman reaction. *ACS Chem Biol* **8**, 749-757 (2013).
- 280 8. X. I. Ambroggio, B. Kuhlman, Computational design of a single amino acid sequence that  
281 can switch between two distinct protein folds. *J Am Chem Soc* **128**, 1154-1161 (2006).
- 282 9. H. K. Privett, G. Kiss, T. M. Lee, R. Blomberg, R. A. Chica, L. M. Thomas, D. Hilvert, K.  
283 N. Houk, S. L. Mayo, Iterative approach to computational enzyme design. *Proc Natl Acad*  
284 *Sci U S A* **109**, 3790-3795 (2012).
- 285 10. G. Bhabha, J. Lee, D. C. Ekiert, J. Gam, I. A. Wilson, H. J. Dyson, S. J. Benkovic, P. E.  
286 Wright, A dynamic knockout reveals that conformational fluctuations influence the  
287 chemical step of enzyme catalysis. *Science* **332**, 234-238 (2011).
- 288 11. J. S. Fraser, M. W. Clarkson, S. C. Degnan, R. Erion, D. Kern, T. Alber, Hidden alternative  
289 structures of proline isomerase essential for catalysis. *Nature* **462**, 669-673 (2009).

- 290 12. S. J. Kerns, R. V. Agafonov, Y. J. Cho, F. Pontiggia, R. Otten, D. V. Pachov, S. Kutter, L.  
291 A. Phung, P. N. Murphy, V. Thai, T. Alber, M. F. Hagan, D. Kern, The energy landscape  
292 of adenylate kinase during catalysis. *Nat Struct Mol Biol* **22**, 124-131 (2015).
- 293 13. S. R. Tzeng, C. G. Kalodimos, Dynamic activation of an allosteric regulatory protein.  
294 *Nature* **462**, 368-372 (2009).
- 295 14. B. D. Allen, A. Nisthal, S. L. Mayo, Experimental library screening demonstrates the  
296 successful application of computational protein design to large structural ensembles. *Proc*  
297 *Natl Acad Sci U S A* **107**, 19838-19843 (2010).
- 298 15. J. A. Davey, R. A. Chica, Improving the accuracy of protein stability predictions with  
299 multistate design using a variety of backbone ensembles. *Proteins* **82**, 771-784 (2014).
- 300 16. J. A. Davey, A. M. Damry, C. K. Euler, N. K. Goto, R. A. Chica, Prediction of Stable  
301 Globular Proteins Using Negative Design with Non-native Backbone Ensembles. *Structure*  
302 **23**, 2011-2021 (2015).
- 303 17. K. A. Crowhurst, S. L. Mayo, NMR-detected conformational exchange observed in a  
304 computationally designed variant of protein Gbeta1. *Protein Eng Des Sel* **21**, 577-587  
305 (2008).
- 306 18. S. Butterworth, V. Lamzin, D. Wigley, J. Derrick, K. Wilson, Anisotropic refinement of a  
307 protein G domain at 1.1 ångstrom resolution. *The Protein Databank in Europe (accessed*  
308 *13.11. 2012)*. Available online at: <http://www.ebi.ac.uk/pdbe>, (1998).
- 309 19. J. P. Derrick, D. B. Wigley, The third IgG-binding domain from streptococcal protein G.  
310 An analysis by X-ray crystallography of the structure alone and in a complex with Fab. *J*  
311 *Mol Biol* **243**, 906-918 (1994).

- 312 20. T. Gallagher, P. Alexander, P. Bryan, G. L. Gilliland, Two crystal structures of the B1  
313 immunoglobulin-binding domain of streptococcal protein G and comparison with NMR.  
314 *Biochemistry* **33**, 4721-4729 (1994).
- 315 21. A. M. Gronenborn, D. R. Filpula, N. Z. Essig, A. Achari, M. Whitlow, P. T. Wingfield, G.  
316 M. Clore, A novel, highly stable fold of the immunoglobulin binding domain of  
317 streptococcal protein G. *Science* **253**, 657-661 (1991).
- 318 22. B. J. Wylie, L. J. Sperl, A. J. Nieuwkoop, W. T. Franks, E. Oldfield, C. M. Rienstra,  
319 Ultrahigh resolution protein structures using NMR chemical shift tensors. *Proc Natl Acad*  
320 *Sci U S A* **108**, 16974-16979 (2011).
- 321 23. J. H. Tomlinson, V. L. Green, P. J. Baker, M. P. Williamson, Structural origins of pH-  
322 dependent chemical shifts in the B1 domain of protein G. *Proteins* **78**, 3000-3016 (2010).
- 323 24. D. J. Wilton, R. B. Tunnicliffe, Y. O. Kamatari, K. Akasaka, M. P. Williamson, Pressure-  
324 induced changes in the solution structure of the GB1 domain of protein G. *Proteins* **71**,  
325 1432-1440 (2008).
- 326 25. P. Strop, A. M. Marinescu, S. L. Mayo, Structure of a protein G helix variant suggests the  
327 importance of helix propensity and helix dipole interactions in protein design. *Protein Sci*  
328 **9**, 1391-1394 (2000).
- 329 26. T. Saio, K. Ogura, M. Yokochi, Y. Kobashigawa, F. Inagaki, Two-point anchoring of a  
330 lanthanide-binding peptide to a target protein enhances the paramagnetic anisotropic effect.  
331 *Journal of biomolecular NMR* **44**, 157-166 (2009).
- 332 27. J. Jee, R. Ishima, A. M. Gronenborn, Characterization of specific protein association by  
333 <sup>15</sup>N CPMG relaxation dispersion NMR: the GB1(A34F) monomer-dimer equilibrium. *J*  
334 *Phys Chem B* **112**, 6008-6012 (2008).

- 335 28. J. Kuszewski, A. M. Gronenborn, G. M. Clore, Improving the packing and accuracy of  
336 NMR structures with a pseudopotential for the radius of gyration. *Journal of the American*  
337 *Chemical Society* **121**, 2337-2338 (1999).
- 338 29. J. R. Lewandowski, M. E. Halse, M. Blackledge, L. Emsley, Protein dynamics. Direct  
339 observation of hierarchical protein dynamics. *Science* **348**, 578-581 (2015).
- 340 30. J. A. Davey, R. A. Chica, Optimization of rotamers prior to template minimization  
341 improves stability predictions made by computational protein design. *Protein Sci* **24**, 545-  
342 560 (2015).
- 343 31. J. K. Myers, C. N. Pace, J. M. Scholtz, Denaturant m values and heat capacity changes:  
344 relation to changes in accessible surface areas of protein unfolding. *Protein Sci* **4**, 2138-  
345 2148 (1995).
- 346 32. I. R. Kleckner, M. P. Foster, An introduction to NMR-based approaches for measuring  
347 protein dynamics. *Biochim Biophys Acta* **1814**, 942-968 (2011).
- 348 33. J. Jee, I. J. Byeon, J. M. Louis, A. M. Gronenborn, The point mutation A34F causes  
349 dimerization of GB1. *Proteins* **71**, 1420-1431 (2008).
- 350 34. E. Campbell, M. Kaltenbach, G. J. Correy, P. D. Carr, B. T. Porebski, E. K. Livingstone,  
351 L. Afriat-Jurnou, A. M. Buckle, M. Weik, F. Hollfelder, N. Tokuriki, C. J. Jackson, The  
352 role of protein dynamics in the evolution of new enzyme function. *Nature chemical biology*  
353 **12**, 944-950 (2016).
- 354 35. Y. Zhang, J. Skolnick, Scoring function for automated assessment of protein structure  
355 template quality. *Proteins* **57**, 702-710 (2004).
- 356 36. J. Skolnick, D. Kihara, Y. Zhang, Development and large scale benchmark testing of the  
357 PROSPECTOR\_3 threading algorithm. *Proteins* **56**, 502-518 (2004).



- 358 37. T. Gallagher, P. Alexander, P. Bryan, G. L. Gilliland, 2 Crystal-Structures of the B1  
359 Immunoglobulin-Binding Domain of Streptococcal Protein-G and Comparison with Nmr.  
360 *Biochemistry*. **33**, 4721-4729 (1994).
- 361 38. Chemical Computing Group Inc. (Chemical Computing Group Inc., 1010 Sherbooke St.  
362 West, Suite #910, Montreal, QC, Canada, H3A 2R7, 2012).
- 363 39. P. Labute, Protonate3D: Assignment of ionization states and hydrogen coordinates to  
364 macromolecular structures. *Proteins-Structure Function and Bioinformatics* **75**, 187-205  
365 (2009).
- 366 40. I. W. Davis, W. B. Arendall, 3rd, D. C. Richardson, J. S. Richardson, The backrub motion:  
367 how protein backbone shrugs when a sidechain dances. *Structure* **14**, 265-274 (2006).
- 368 41. F. Lauck, C. A. Smith, G. F. Friedland, E. L. Humphris, T. Kortemme, RosettaBackrub-a  
369 web server for flexible backbone protein structure modeling and design. *Nucleic Acids*  
370 *Research* **38**, W569-W575 (2010).
- 371 42. S. G. Nash, A survey of truncated-Newton methods. *J. Comput. Appl. Math.* **124**, 45-59  
372 (2000).
- 373 43. J. Wang, P. Cieplak, P. A. Kollman, How well does a restrained electrostatic potential  
374 (RESP) model perform in calculating conformational energies of organic and biological  
375 molecules? *Journal of Computational Chemistry* **21**, 1049-1074 (2000).
- 376 44. R. A. Chica, M. M. Moore, B. D. Allen, S. L. Mayo, Generation of longer emission  
377 wavelength red fluorescent proteins using computationally designed libraries. *Proc Natl*  
378 *Acad Sci U S A* **107**, 20257-20262 (2010).
- 379 45. B. D. Allen, S. L. Mayo, Dramatic performance enhancements for the FASTER  
380 optimization algorithm. *J Comput Chem* **27**, 1071-1075 (2006).

- 381 46. B. D. Allen, S. L. Mayo, An efficient algorithm for multistate protein design based on  
382 FASTER. *J Comput Chem* **31**, 904-916 (2010).
- 383 47. R. L. Dunbrack, F. E. Cohen, Bayesian statistical analysis of protein side-chain rotamer  
384 preferences. *Protein Science* **6**, 1661-1681 (1997).
- 385 48. S. L. Mayo, B. D. Olafson, W. A. Goddard, Dreiding - a Generic Force-Field for Molecular  
386 Simulations. *J. Phys. Chem.* **94**, 8897-8909 (1990).
- 387 49. B. I. Dahiyat, S. L. Mayo, Probing the role of packing specificity in protein design. *Proc*  
388 *Natl Acad Sci U S A* **94**, 10172-10177 (1997).
- 389 50. T. Lazaridis, M. Karplus, Discrimination of the native from misfolded protein models with  
390 an energy function including implicit solvation. *Journal of Molecular Biology* **288**, 477-  
391 487 (1999).
- 392 51. E. K. Koepf, H. M. Petrassi, M. Sudol, J. W. Kelly, WW: An isolated three-stranded  
393 antiparallel beta-sheet domain that unfolds and refolds reversibly; evidence for a structured  
394 hydrophobic cluster in urea and GdnHCl and a disordered thermal unfolded state. *Protein*  
395 *Science : A Publication of the Protein Society* **8**, 841-853 (1999).
- 396 52. F. Delaglio, S. Grzesiek, G. W. Vuister, G. Zhu, J. Pfeifer, A. Bax, NMRPipe: A  
397 multidimensional spectral processing system based on UNIX pipes. *Journal of*  
398 *biomolecular NMR* **6**, 277-293 (1995).
- 399 53. B. A. Johnson, R. A. Blevins, NMR View: A computer program for the visualization and  
400 analysis of NMR data. *Journal of biomolecular NMR* **4**, 603-614 (1994).
- 401 54. D. Wishart, B. Sykes, F. Richards, The chemical shift index: a fast and simple method for  
402 the assignment of protein secondary structure through NMR spectroscopy. *Biochemistry*  
403 **31**, 1647-1651 (1992).

- 404 55. N. A. Farrow, O. Zhang, J. D. Forman-Kay, L. E. Kay, A heteronuclear correlation  
405 experiment for simultaneous determination of <sup>15</sup>N longitudinal decay and chemical  
406 exchange rates of systems in slow equilibrium. *Journal of biomolecular NMR* **4**, 727-734  
407 (1994).
- 408 56. Y. Shen, F. Delaglio, G. Cornilescu, A. Bax, TALOS+: a hybrid method for predicting  
409 protein backbone torsion angles from NMR chemical shifts. *Journal of biomolecular NMR*  
410 **44**, 213-223 (2009).
- 411 57. P. Güntert, in *Protein NMR Techniques*, A. K. Downing, Ed. (Humana Press, Totowa, NJ,  
412 2004), pp. 353-378.
- 413 58. C. A. Smith, T. Kortemme, Predicting the tolerated sequences for proteins and protein  
414 interfaces using RosettaBackrub flexible backbone design. *PloS one* **6**, e20451 (2011).
- 415 59. J. A. Davey, R. A. Chica, Multistate Computational Protein Design with Backbone  
416 Ensembles. *Methods Mol Biol* **1529**, 161-179 (2017).
- 417 60. I. W. Davis, A. Leaver-Fay, V. B. Chen, J. N. Block, G. J. Kapral, X. Wang, L. W. Murray,  
418 W. B. Arendall, 3rd, J. Snoeyink, J. S. Richardson, D. C. Richardson, MolProbity: all-atom  
419 contacts and structure validation for proteins and nucleic acids. *Nucleic Acids Res* **35**,  
420 W375-383 (2007).
- 421 61. A. Bhattacharya, R. Tejero, G. T. Montelione, Evaluating protein structures determined by  
422 structural genomics consortia. *Proteins: Structure, Function, and Bioinformatics* **66**, 778-  
423 795 (2007).
- 424 62. Y. J. Huang, R. Powers, G. T. Montelione, Protein NMR Recall, Precision, and F-measure  
425 Scores (RPF Scores): Structure Quality Assessment Measures Based on Information  
426 Retrieval Statistics. *Journal of the American Chemical Society* **127**, 1665-1674 (2005).

427

428 **Supplementary Materials:**

429 Supplementary Text

430 Figs. S1 to S16

431 Tables S1 to S4

432

433 **Acknowledgments**

434 R.A.C. acknowledges grants from the Natural Sciences and Engineering Research Council of  
435 Canada (NSERC), the Ontario Research Fund, and the Canada Foundation for Innovation. N.K.G.  
436 acknowledges a grant from NSERC. J.A.D. is the recipient of an Ontario Graduate Scholarship and  
437 A.M.D. is the recipient of a NSERC postgraduate scholarship. We acknowledge Dr. Glenn Facey,  
438 Dr. Yves Aubin, and Simon Sauvé for assistance with NMR experiments, as well as Dr. Yun Mou  
439 for helpful discussions.

440

441 **Author Contributions**

442 J.A.D. and A.M.D. performed the experiments and analyzed data. N.K.G. and A.M.D. designed  
443 NMR experiments and analyzed data. J.A.D. and R.A.C. designed computational experiments. All  
444 authors wrote the manuscript.

445

446

447 **Table 1.** Predicted and Experimental Properties of G $\beta$ 1 variants

Protein	Mutations	Meta-MSD Predictions			Stability	Exchange <sup>e</sup>			
		Behavior <sup>a</sup>	$\Delta E_{eq}$ <sup>b</sup> (kcal/mol)	$\Delta E^\ddagger$ <sup>c</sup> (kcal/mol)	$\Delta G_U$ <sup>d</sup> (kcal/mol)	$k_{-1}$ <sup>f</sup> (s <sup>-1</sup> )	$k_1$ <sup>g</sup> (s <sup>-1</sup> )	$\Delta G^\ddagger$ <sup>h</sup> (kcal/mol)	$\Delta G_{eq}$ <sup>i</sup> (kcal/mol)
Wild type		+g(-)	8.6	15.2	4.1 ± 0.2				
DANCER-0	Y3F/L5A/L7I/A34F/V39I	-g(+) ↔ -g(-)	0.9	7.8	1.5 ± 0.2				
DANCER-1	Y3F/L5A/L7I/A34F/V39L/V54I	-g(-) ↔ -g(+)	3.7	8.4	2.2 ± 0.1	30 ± 10	110 ± 50	18.9 ± 0.3	0.3 ± 0.1
DANCER-2	Y3F/L5A/L7I/A34F/V39L	-g(+) ↔ -g(-)	1.3	9.4	1.7 ± 0.1	j	j	j	1.4 ± 0.7
DANCER-3	Y3F/L7I/A34F/V39L/V54I	-g(-) ↔ -g(+)	2.9	13.7	2.0 ± 0.3	3.9 ± 0.2	23 ± 5	20.65 ± 0.08	1.3 ± 0.3
NERD-S	Y3F/L7I/A34F/V39I/V54I	-g(+)	4.3	14.7	2.7 ± 0.1				
NERD-C	Y3F/L7I/F30L/V39I	+g(-)	12.2	15.3	4.0 ± 0.3				

448 <sup>a</sup> Static variants (NERD-S and NERD-C) are predicted to occupy a single state while DANCER proteins are predicted to exchange between major and minor states (major state ↔

449 minor state)

450 <sup>b</sup> Energy difference between the two lowest energy states

451 <sup>c</sup> Energy barrier to conformational exchange (see SI text for more detail)

452 <sup>d</sup> Free energy of unfolding determined by chemical denaturation with guanidium chloride at 25 °C

453 <sup>e</sup> Kinetic parameters ( $k_1$ ,  $k_{-1}$ ,  $\Delta G^\ddagger$ ) reported at 15 °C,  $\Delta G_{eq}$  at 25 °C.

454 <sup>f</sup> Rate constant for exchange from major to minor state

455 <sup>g</sup> Rate constant for exchange from minor to major state

456 <sup>h</sup> Energy barrier for exchange from major to minor state

457 <sup>i</sup> Free energy difference between major and minor states

458 <sup>j</sup> Exchange peaks were observed but could not be quantified

459 **Table 2.** Comparison of predicted and experimental structures

<b>Protein</b>	<b>TM-score to 1PGA<sup>a</sup></b>	<b>Predicted Trp43 Conformation</b>	<b>Experimental <math>\chi_1</math> (°)</b>	<b>Experimental <math>\chi_2</math> (°)</b>
<b>DANCER-2</b>				
Major species	0.67	-g(+)	+75 ± 2	-74 ± 1
Minor Species	0.66	-g(-)	-95 ± 1	-110 ± 2
<b>Static G<math>\beta</math>1 variants</b>				
NERD-S	0.66	-g(+)	+54 ± 4	-89 ± 2
NERD-C	0.85	+g(-)	-84 ± 4	+80 ± 4

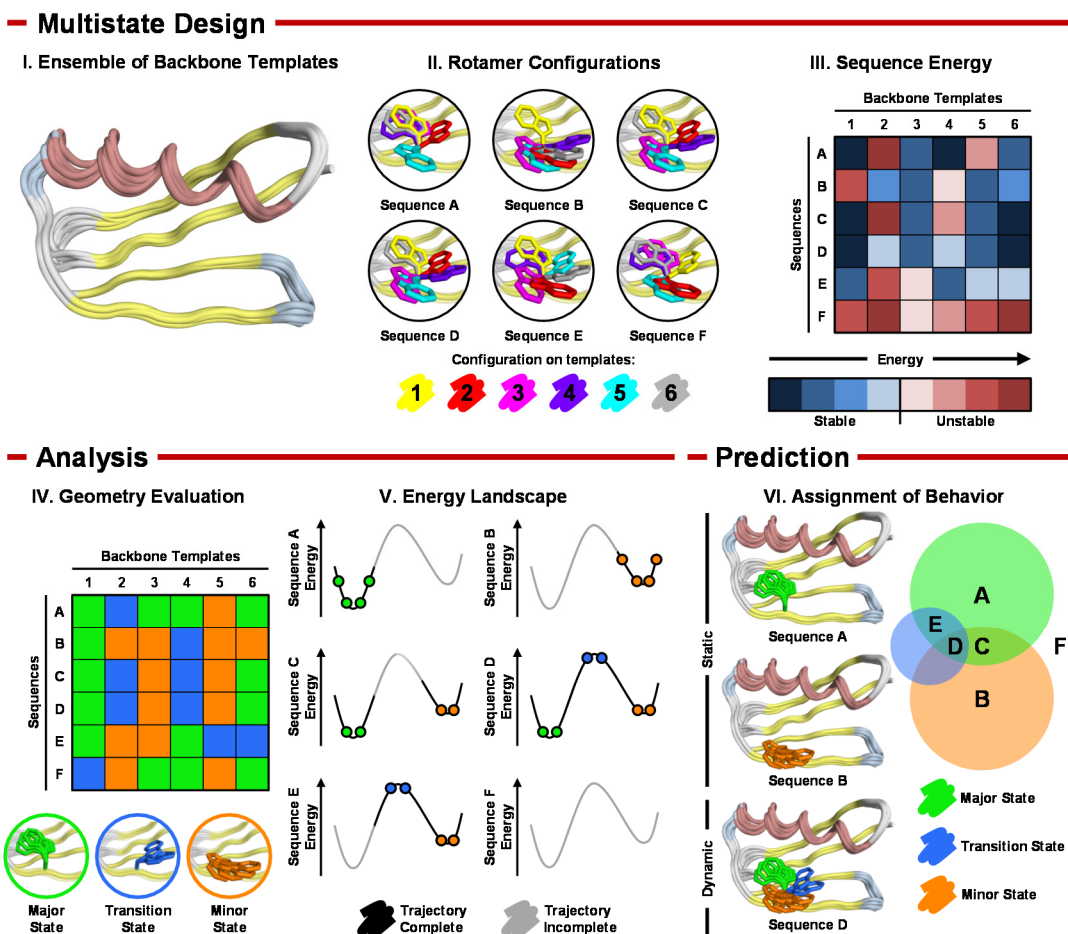
460

461 <sup>a</sup> TM-score has a value between 0 and 1, where 1 indicates a perfect match between two structures. Two proteins with a TM-score

462 greater than 0.5 are considered to adopt the same fold (35, 36).

463

464 **Figures**



465

466

467 **Figure 1. Meta-MSD.** Multistate design (MSD) with an ensemble of backbone templates

468 approximating the conformational landscape for dynamic exchange between targeted states (I) is

469 used to generate microstates by solving the lowest energy rotamer configuration for each sequence

470 on each backbone template (II). MSD also returns an energy value for each microstate that reflects

471 its predicted stability (III). A geometry-based analysis of the rotamer-optimized microstates is

472 performed (IV), allowing assignment of each microstate to major, minor or transition state in the

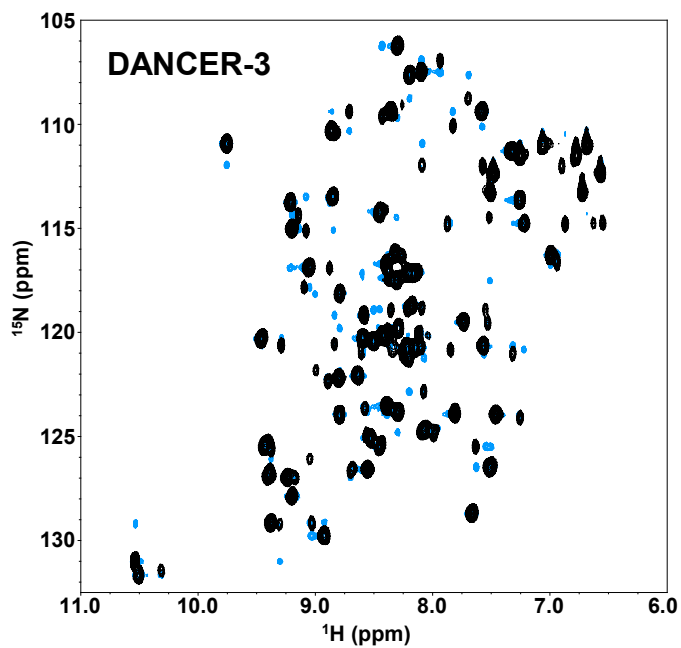
473 energy landscape (V). Prediction of conformational dynamics is then done based on an evaluation

474 of the relative energies of these states (VI). For a sequence to be predicted as dynamic, all three

475 states must be stable, with an energy profile that is compatible with exchange (e.g., sequence D).  
476 Sequences A, B, and C are predicted to be static because they either stabilize a single state or cannot  
477 stabilize the transition state required for exchange. Sequence E is also predicted to be static because  
478 it stabilizes only one endpoint state. Sequence F is predicted to be unfolded because it is unstable  
479 on all states.  
480



481



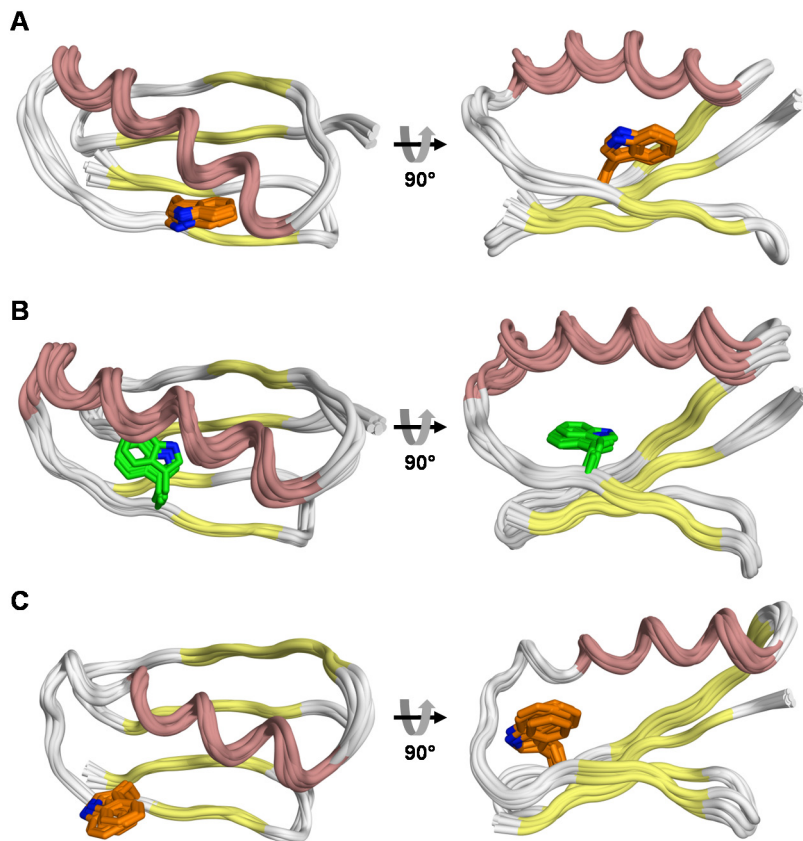
482

483

484 **Figure 2.**  $^1\text{H}$ - $^{15}\text{N}$  ZZ-Exchange spectrum for DANCER-3. ZZ-Exchange spectrum (blue) is  
485 shown overlaid with  $^1\text{H}$ - $^{15}\text{N}$  HSQC spectrum (black) to highlight the presence of exchange peaks.

486

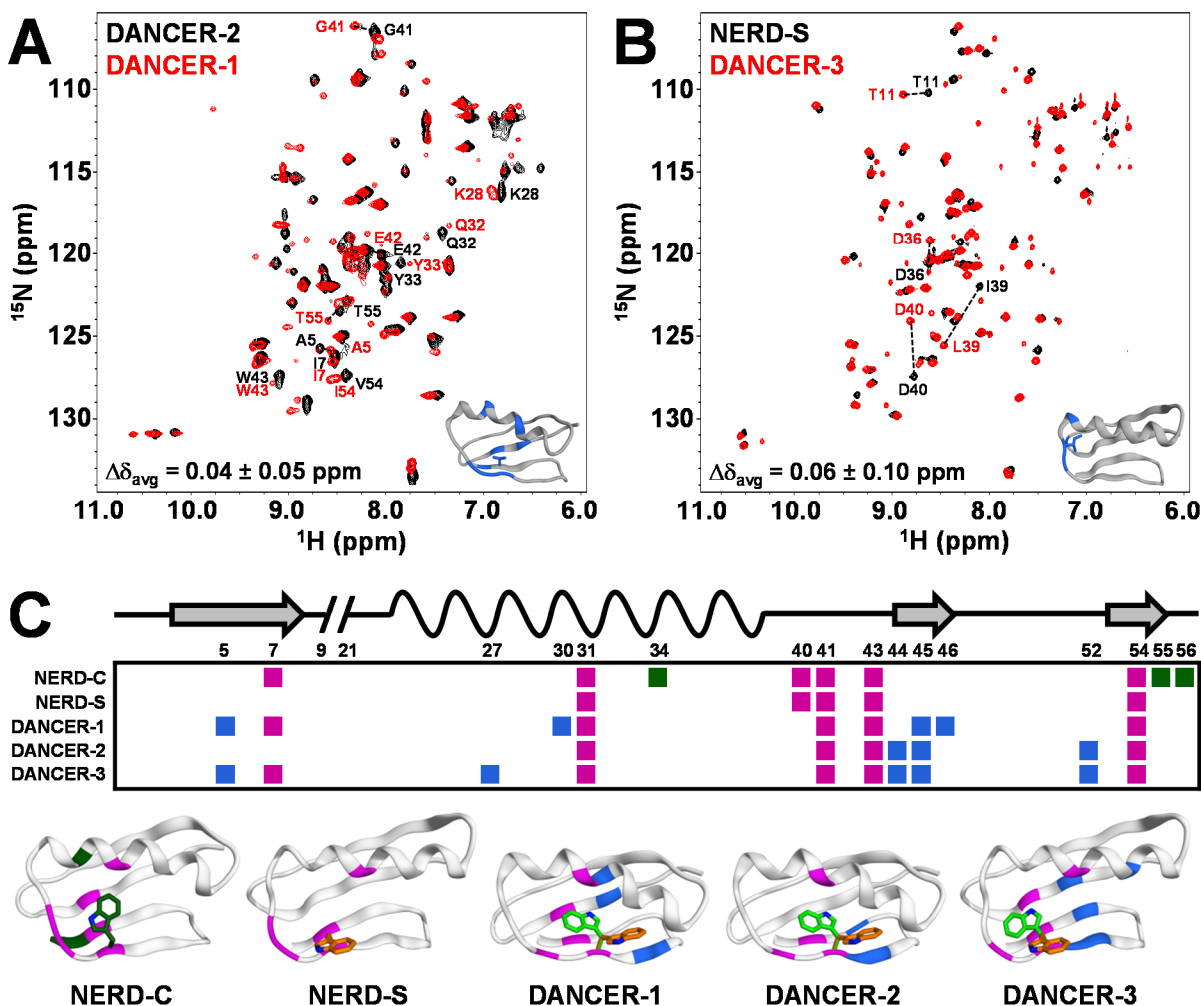
487



488  
489 **Figure 3. Solution structures of Gβ1 variants.** NMR ensembles for (A) DANCER-2 major  
490 species, (B) DANCER-2 minor species, and (C) NERD-S. The minor species of DANCER-2 is a  
491 model generated using NOESY data that excluded a small subset of peaks from the automatic NOE  
492 assignment process that could be unambiguously assigned to the major species (SI Text). The  
493 Trp43 side chain is shown as sticks.

494

495



496  
 497 **Figure 4. Structural analysis of DANCER-1 and DANCER-3.** (A) Superimposed  $^1\text{H}$ - $^{15}\text{N}$ -HSQC  
 498 spectra of DANCER-2 and DANCER-1 reveal high structural similarity between major states.  
 499 Residues showing significant average amide shift differences ( $\Delta\delta > \Delta\delta_{\text{avg}} + 1\sigma$ ) are labeled and  
 500 highlighted in blue on the inset DANCER-2 structure. These residues are all proximal to the single  
 501 amino acid that differs between the two DANCER proteins (shown as sticks). (B)  $^1\text{H}$ - $^{15}\text{N}$ -HSQC  
 502 spectra demonstrating that the major state of DANCER-3 has the same structure as NERD-S. (C)  
 503 Summary of NOE correlations involving the Trp43 indole N-H shown on a position map  
 504 (secondary structure elements on top) and on each structure. Correlations are colored green, blue,  
 505 or magenta, if they are observed in static, dynamic, or both variants respectively. Trp43 side-chain

506 conformation(s) consistent with observed NOEs are shown for each structure. Included in this  
507 analysis is the solution NMR structure of NERD-C (*Non-Exchanging Rigid Design with a Core-*  
508 *buried* Trp43 conformation, SI Text), which adopts the native +g(-) configuration (Fig. S15, Table  
509 2). NERD-C shows several unique indole N-H NOE correlations that are not observed in any of  
510 the DANCER variants, confirming that this state is not sampled by the DANCER proteins.  
511